Giant Shape-Persistent Tetrahedral Porphyrin System: Light-Induced Charge Separation

Marianna Marchini,[a] Alessandra Luisa,[b] Giacomo Bergamini,[a] Nicola Armaroli,[c] Barbara Ventura,*[c] Massimo Baroncini,*[a, d] Nicola Demitri,[e] Elisabetta Iengo,*[b] and Paola Ceroni*[a]

Dedicated to Professor Vincenzo Balzani on the occasion of his 85th birthday.

Abstract: Tetraphenylmethane appended with four pyridyl-pyridinium units works as a scaffold to self-assemble four ruthenium porphyrins in a tetrahedral shape-persistent giant architecture. The resulting supramolecular structure has been characterised in the solid state by X-ray single crystal analysis and in solution by various techniques. Multinuclear NMR spectroscopy confirms the 1:4 stoichiometry with the formation of a highly symmetric structure. The self-assembly process can be monitored by changes of the redox potentials, as well as by modifications in the visible absorption spectrum of the ruthenium porphyrin and by a complete quenching of both the bright fluorescence of the tetracationic scaffold and the weak phosphorescence of the ruthenium porphyrin. An ultrafast photoinduced electron transfer is responsible for this quenching process. The lifetime of the resulting charge separated state (800 ps) is about four times longer in the giant supramolecular structure compared to the model 1:1 complex formed by the ruthenium porphyrin and a single pyridylpyridinium unit. Electron delocalization over the tetrameric pyridinium structure is likely to be responsible for this effect.

Introduction

The study of multichromophoric systems with a shape-persistent arrangement of the chromophores has gained increasing relevance:[1] new properties may emerge from the interaction between the units and a precise control of the interchromophoric units is assured by the shape-persistent structure, on the contrary to multichromophoric systems based on polymeric scaffolds. These systems are thus expected to have potential applications in the fields of supramolecular chemistry, luminescent sensors with signal amplification, light-harvesting antennae and material science.[2]

Pyridinium and bipyrididium chromophores (also known as viologens, namely, 1,1′-disubstituted-4,4-bipyridinium salts) are extensively studied organic fragments due to their photochemical and electrochemical properties.[3] They are widely employed as electron-acceptor recognition sites and redox switching units in supramolecular systems such as dendrimers,[4–8] rotaxanes,[9,10] and catenanes.[11,12] Moreover, they have been investigated as components for electrochromic displays, molecular batteries, redox mediators, and redox

[a] Dr. M. Marchini, Prof. G. Bergamini, Dr. M. Baroncini, Prof. P. Ceroni
Department of Chemistry Giacomo Ciamician
University of Bologna
Via Selmi 2, 40126 Bologna (Italy)
E-mail: paola.ceroni@unibo.it
        massimo.baroncini@unibo.it

[b] Dr. A. Luisa, Prof. Dr. E. Iengo
Department of Chemical and Pharmaceutical Sciences
University of Trieste
Via L. Giorgieri 1, 34127 Trieste (Italy)
E-mail: eiengo@units.it

[c] Dr. N. Armaroli, Dr. B. Ventura
Istituto per la Sintesi Organica e la Fotoreattività
Consiglio Nazionale delle Ricerche (ISOF-CNR)
Via P. Gobetti 101, 40129 Bologna (Italy)
E-mail: barbara.ventura@isof.cnr.it

[d] Dr. M. Baroncini
Dipartimento di Scienze e Tecnologie Agro-Alimentari
Università di Bologna
Viale Fanin 44, 40127 Bologna (Italy)

and
CLAN-Center for Light Activated Nanostructures
ISOF-CNR
Via Gobetti 101, 40129 Bologna (Italy)

[e] Dr. N. Demitri
Elettra-Sincrotrone Trieste
S.S. 14 Km 163.5 in Area Science Park, 34149 Basovizza-Trieste (Italy)

Chemistry–A European Journal

Full Paper
doi.org/10.1002/chem.202102135

Chemistry
Europe
European Chemical
Societies Publishing

sensors.[13–15] Concurrently, tetraphenylmethane is one of the most exploited divergent synthons, used as precursor for the preparation of shape-persistent structures.[16–19] On the other hand, ruthenium porphyrins are known to bind to pyridyl units with strong and inert Ru–N bond formation.[20] This recognition motif has been widely applied for the construction of photo- and redox-active supramolecular systems.[21]

Results and Discussion

The supramolecular tetrahedral multiporphyrin system 1^{4+} ⊃4Ru(CO)FTPP (see Scheme S1), self-assembled from a tetra-fluorinated ruthenium porphyrin and a shape-persistent structure based on pyridylpyridium units (Ru(CO)FTPP and 1^{4+}, respectively, Scheme 1), was prepared and studied. The association of a pyridyl phenyl-pyridinium unit (2^+, Scheme 1) and the same ruthenium porphyrin was used as a model system (see Scheme S1).[22]

In all cases, the assembling process proceeds almost quantitatively under mild experimental conditions (see Schemes S1–S2, and Experimental Section): the self-assembled systems 2^+⊃Ru(CO)FTPP and 1^{4+}⊃4Ru(CO)FTPP, together with the structurally related conjugates,[22] can be obtained in acetone by stirring (for 30 minutes) either the model compound 2^+ or the tetramer 1^{4+}, as hexafluorophostate salts,[23] with one equivalent of metalloporphyrin per pyridine moiety, followed by precipitation of the corresponding product by addition of n-hexane (yield 80%–90%). High-resolution ^1H and ^{19}F NMR experiments were chosen for the solution characterization of these adducts, since the inert, and relatively strong nature of the ruthenium-nitrogen bond provides clear spectra with sharp resonances (full and unambiguous 1D and 2D NMR solution characterization of all derivatives[22] can be found in the Supporting Information). Moreover, the large aromatic core of the porphyrin(s) induces, in general, a very characteristic and diagnostic shielding effect on the active nuclei of the axially coordinated ligand (on the contrary, the resonances of the metallo-porphyrin(s) are not particularly affected by axial coordination to the metal center).[20a,d,21,24] Given that the single building components and the assembled systems are in slow

exchange with respect to the NMR timescale, and spread over a large chemical shift range, the self-assembling process is relatively easy to monitor. In fact, the target species[22] appears as a set of sharp resonances well distinguishable from those of the free components. In particular, the tetrahedral system 1^{4+} exhibits four binding sites, so four equivalents of Ru(CO)FTPP were progressively added to a 1^{4+} acetone-d_6 solution. Before the stoichiometric ratio between the two units is reached, the 1D NMR spectra appears as quite crowded with different sets of resonances, as a consequence of the co-existence of non-equilibrating partially assembled intermediate species. When the 1:4 stoichiometry between 1^{4+} and Ru(CO)FTPP is reached, the spectra simplify considerably (see Figures 1, S3 and S5) and the following observations can be made:
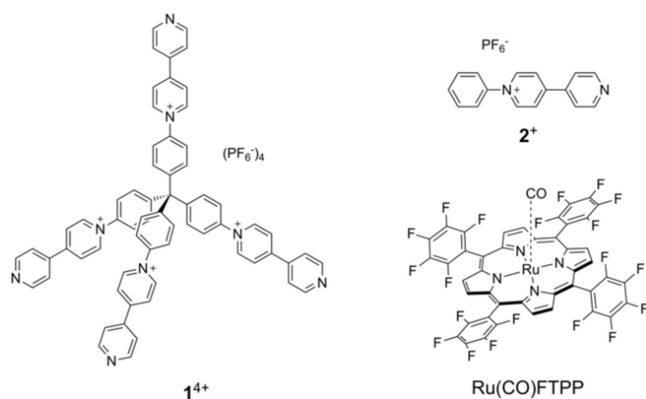
i) The presence of only one set of signals is consistent with the presence of a highly symmetrical system; ii) ^1H and ^{19}F signal relative integrations confirms the 1:4 stoichiometry; iii) individual resonances of all five fluorine atoms of the *meso*-pentafluorophenyl groups are found in the ^{19}F NMR spectra (with the correct F–F coupling), with a significant inequivalence of the *ortho*F and *metha*F, both giving rise to two well separated sets of multiplets (Figure S5).[25]

As expected, coordination of the pyridyl groups to the ruthenium center is accompanied by strong upfield shifts of the proton resonances of the 1^{4+} axial ligand, with this effect being progressively less dramatic as the distance from the perpendicular porphyrin aromatic macrocycle increases (Figure 1). All these spectral features, also in comparison with those found for the model system 2^+⊃Ru(CO)FTPP and the related derivatives[22] (see also Figures S1–S13 in the Supporting Information), are in perfect agreement with the unique formation of a symmetrical shape-persistent tetrahedral array, namely $[1^{4+}$⊃4Ru(CO)FTPP][PF$_6$]$_4$, in which four ruthenium-porphyrins are pinpointed at the periphery of the central 1^{4+} scaffold, by axial coordination of each of the four pyridyl arms to one ruthenium center.
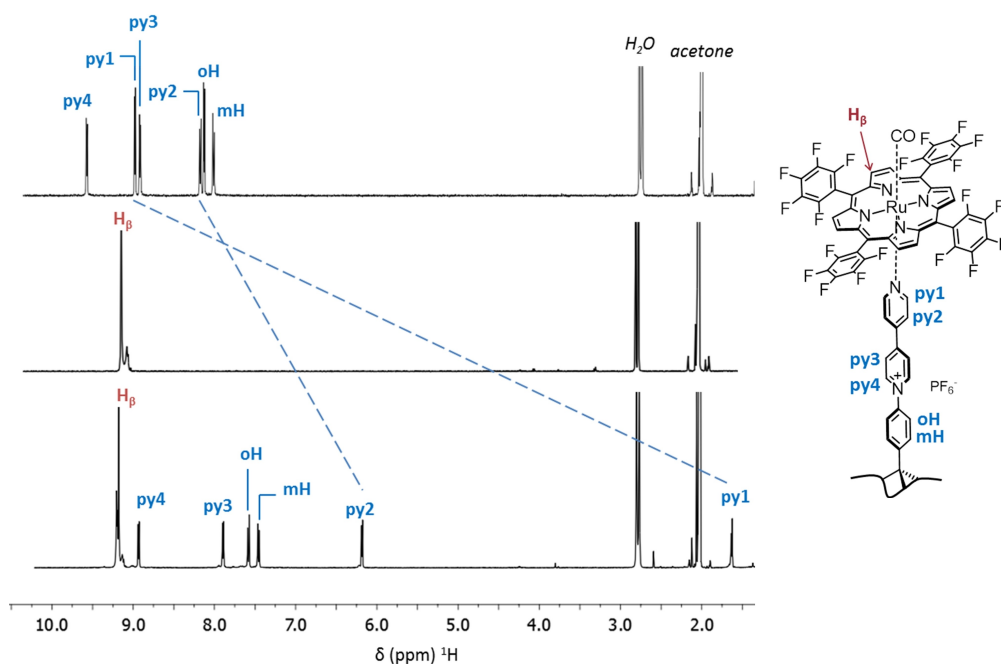
To recover additional information on the size of the assembly, DOSY experiments on the full series of conjugates[22] were performed. The 2D ^1H-DOSY maps for Ru(CO)FTPP, 1^{4+} (Figure 2, blue) and the assembled system 1^{4+}⊃4Ru(CO)FTPP (Figure 2, dark red) are reported in Figure 2. The average *Diffusion Coefficients* (D_t) obtained for 1^{4+}, 2^+, the Ru^{II}(CO)-porphyrin units, the model compounds and the tetrahedral assemblies (obtained by mono-exponential fitting of the ^1H signals intensity decays) are reported in Table S1. They show a nice correlation between the decrease of the D_t values when the dimensions of the conjugates increase.

Finally, in a 2D HF-HOESY experiment weak, but distinct, through-space cross-peaks between the fluorines signals of PF$_6^-$ and the protons of the phenyl-pyridinium portions of 1^{4+} can be found, indicating that, at least in acetone and on the NMR time-scale, the oppositely charged counterparts are in relatively close spatial proximity (Figure S6).[26]

Single crystals suitable for X-ray analysis were obtained for $[1^{4+}$⊃4Ru(CO)FTPP][PF$_6$]$_4$ and the model compounds $[2^+$⊃Ru(CO)FTPP][PF$_6$] and $[2^+$⊃Ru(CO)OEP][PF$_6$][22] by slow vapour diffusion of n-hexane over concentrated acetone solutions. In

Scheme 1. Chemical structure of the building units 1^{4+}, 2^+ and Ru(CO)FTPP.

Chemistry–A European Journal
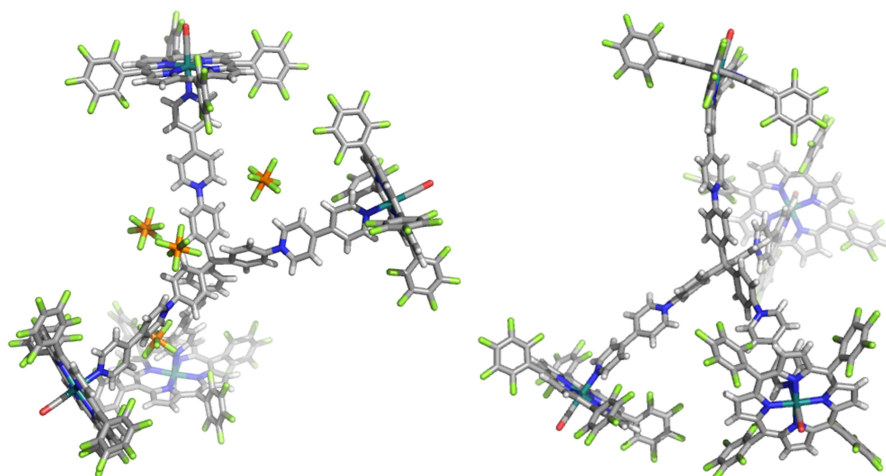
Full Paper
doi.org/10.1002/chem.202102135

Chemistry Europe
European Chemical
Societies Publishing

Figure 1. ^{1}H NMR spectra (acetone-d_6, 500 MHz) of $\mathbf{1^{4+}}$ (top), Ru(CO)FTPP (center) and assembled system $\mathbf{1^{4+}}{\supset}4$Ru(CO)FTPP, after addition of four equivalents of Ru(CO)FTPP (bottom). Dashed lines highlight the resonances for the proton signals of the scaffold with the largest observed upfield shifts. For simplicity, only one of the four arms is depicted, with proton labelling scheme.
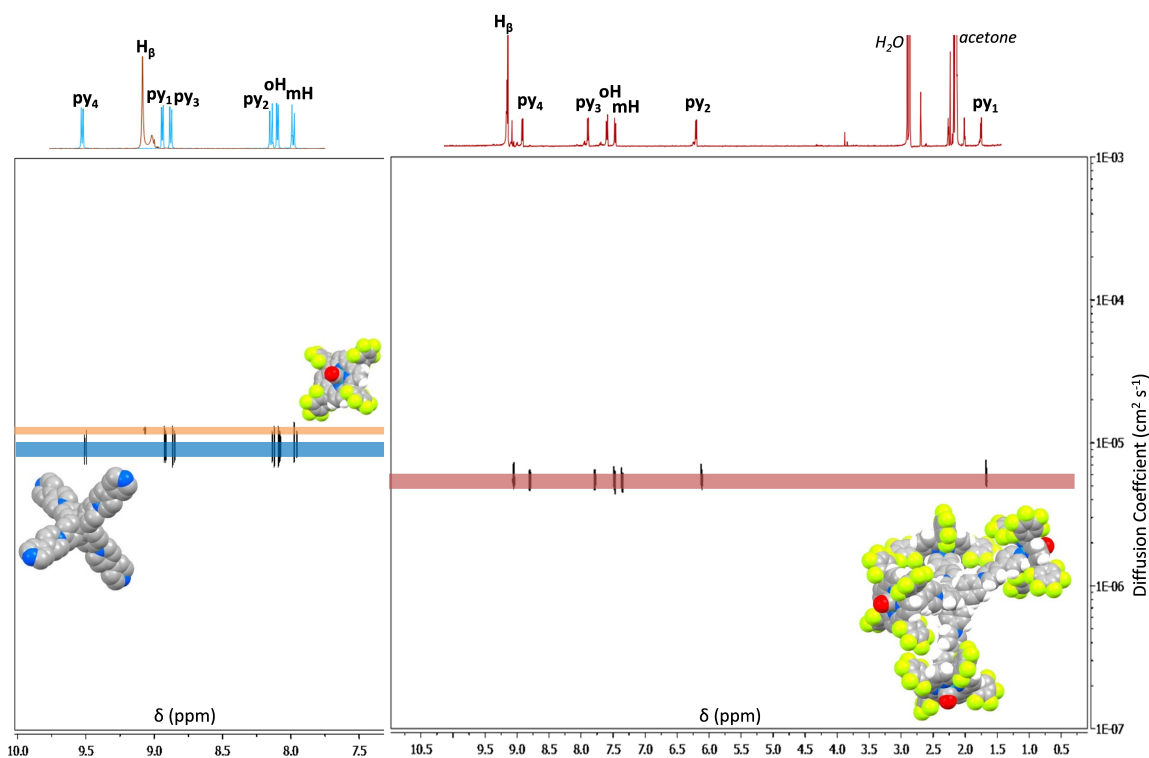
Figure 2. Comparison between 2D ^{1}H-DOSY spectra (Bayesian transform, acetone-d6, 500 MHz) of Ru(CO)FTPP (orange), $\mathbf{1^{4+}}$ (blue) and the assembled system $\mathbf{1^{4+}}{\supset}4$Ru(CO)FTPP (dark red). On the horizontal axes, the 1D ^{1}H spectrum for the components and the assembly are reported. The different species are depicted with a space-fill representation (colour code: C, Ru grey; H, white; N, blue; F, light green; O, red).

agreement with what found in solution by NMR (see above), $\mathbf{1^{4+}}{\supset}4$Ru(CO)FTPP consists of a giant assembly, containing four

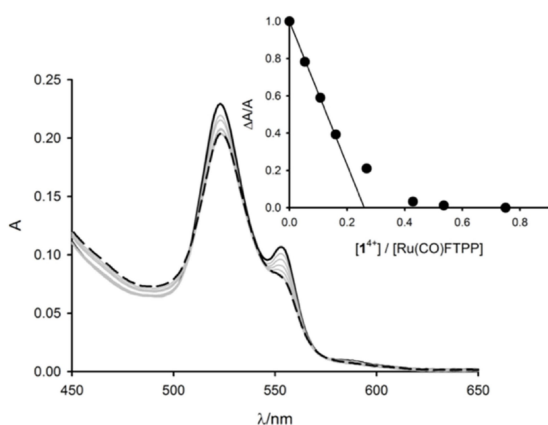metalloporphyrins at the periphery of the tetra-cationic $\mathbf{1^{4+}}$ scaffold (Figure 3). The central tetrahedral system $\mathbf{1^{4+}}$ presents

16252

Chemistry–A European Journal

Full Paper
doi.org/10.1002/chem.202102135

Chemistry Europe
European Chemical
Societies Publishing

Figure 3. Two views of the X-ray structure of [1^{4+}⊃4Ru(CO)FTPP][PF$_6$]$_4$ (stick representation; PF$_6^-$ anions are omitted on the right side; colour code: C, grey; H, white; F light green; Ru, dark green; O, red; P, orange).

a distorted structure, compressed on two sides, with the closer and the wider apart pyridylpyridinium arms defining, respectively, ca. 85° and 126° angles. As a result, the peripheral Ru(CO) FTPP units are pinpointed at the vertexes of a tetrahedron with sides of unequal lengths (24.2 Å is the expected for the Ru…Ru distance in an ideal tetrahedron with internal angles of 109.47°, while distances spanning from 26.8 Å to 18.6 Å are found, Figure S19). The severe distortions found in the solid state, as opposite to the presence of a highly symmetrical array detected in solution (see above) can very likely be ascribed to an averaged contribution of intra- and inter-molecular charge repulsions. A total of two ordered PF$_6^-$ anions can be localized in between the closer 1^{4+} arms, with the shortest F···N$^+$ distance being of 3.83 Å, while two heavily disordered anions are found in between the opened arms space. An approximate crystallographic radius r_{XRD} of ca. 16 Å can be calculated for [1^{4+}
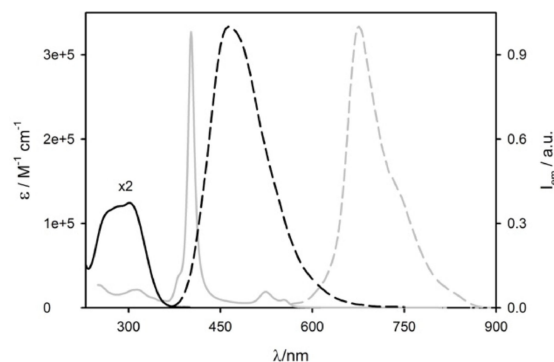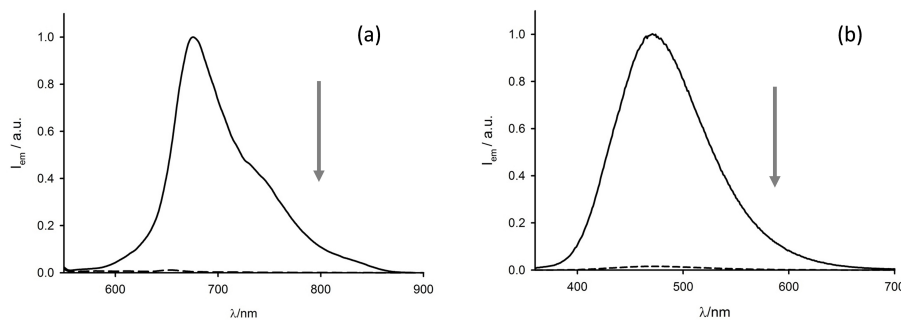

Figure 4. Absorption (solid lines) and normalised emission spectra (dashed lines) of 1^{4+} (black lines) and Ru(CO)FTPP (grey lines) in acetonitrile and CH$_2$Cl$_2$ respectively at 298 K. The normalised phosphorescence of the Ru(CO) FTPP was measured in deaerated solution. Optical path length 1 cm.

⊃4Ru(CO)FTPP][PF$_6$]$_4$, by considering the external oxygen atoms of the -CO moieties as positioned in an ideal sphere surface. The corresponding hydrodynamic radius in solution, derived from the ^{1}H DOSY analysis (r_H = 12.8 Å, see Table S1), has a value of about the 80% of the crystallographic one, in line with the indications reported in the literature.[27] Additional details, together with the structural analysis of the model systems, are provided in the X-ray analysis and Structural Characterization Section of the Supporting Information.

The photophysical properties of the building blocks 1^{4+} and Ru(CO)FTPP were investigated in acetonitrile and dichloromethane solutions, respectively (Figure 4).[22] The tetramer shows an absorption band in the UV region of the spectrum with maximum at 302 nm, and exhibits a very intense blue emission band at 464 nm (Φ_{em} = 40%, τ = 1.0 ns in acetonitrile),[28] compared to the model compound 2^+ that shows extremely weak emission (Φ_{em} = 0.4%, τ = 0.2 ns in acetonitrile) centred at 431 nm.[29] The absorption spectrum of the ruthenium porphyrin Ru(CO)FTPP shows an intense Soret band at 402 nm and two Q-bands at 524 and 555 nm. Ru(CO)

Figure 5. Absorption spectra of the enlarged Q-bands region recorded after increasing amount of 1^{4+} (up to 0.78 equivalents) to a Ru(CO)FTPP dissolved in acetone: the black solid line is the absorption spectrum of the free porphyrin in solution; the black dashed line is the spectrum recorder after the addition of 0.78 equivalents of 1^{4+}. Inset: normalized absorption changes at 525 nm upon addition of 1^{4+}.

Chemistry–A European Journal

Full Paper
doi.org/10.1002/chem.202102135

**Chemistry
Europe**
European Chemical
Societies Publishing

Figure 6. Phosphorescence emission spectra (λ_{exc} 530 nm, delay time 0.01 ms) of free ruthenium porphyrin in de-oxygenated CH_2Cl_2 (black solid line, plot a) solution and after the addition of an excess of $\mathbf{1}^{4+}$, added from acetone (black dashed line, plot a) at room temperature. Fluorescence spectra (λ_{exc} 330 nm) of the free $\mathbf{1}^{4+}$ in acetone solution (black solid line, plot b) and after addition of an excess of ruthenium porphyrin (black dashed line, plot b). The arrows indicate the decrease of the emission intensity caused by the quenching process.

FTPP is weakly emissive in deareated dichloromethane solution, with a maximum at 676 nm ($\Phi_{em} = 0.09\%$, $\tau = 0.012$ ms). After having determined the photophysical features of the individual moieties $\mathbf{1}^{4+}$ and Ru(CO)FTPP, spectrophotometric titrations were performed to trace the formation of the supramolecular assembly. Titration experiments were performed in acetone, a less-coordinating solvent compared to acetonitrile, so that a higher association constant is expected.

Upon addition of increasing amounts of $\mathbf{1}^{4+}$ to a solution of Ru(CO)FTPP in acetone, the absorption spectrum of the Ru(CO) FTPP is slightly modified. The Soret-band is red-shifted (Figure S20) while the Q-bands decrease in intensity (Figure 5). The 1:4 stoichiometry of the adduct $\mathbf{1}^{4+} \supset 4$Ru(CO)FTPP is confirmed by the observed absorbance changes, which can be extrapolated to 0.25 equivalent of tetramer per Ru(CO)FTPP (Figure 5, inset). The weak Ru(II) porphyrin phosphorescence is completely quenched (Figure 6a) when an excess of tetramer is added in solution.

On the other hand, when an excess of ruthenium porphyrin is added to a $\mathbf{1}^{4+}$ solution, a complete quenching of the tetramer fluorescence is observed (Figure 6b; see Supporting Information for more details).

Therefore, in the supramolecular adduct $\mathbf{1}^{4+} \supset 4$Ru(CO)FTPP, the luminescence of both components is completely quenched at room temperature.

Conversely, at 77 K no quenching of the Ru(II) porphyrin phosphorescence is detected, even when an excess of tetramer is added in solution (Figure S24): the excited state lifetime is the same of the free porphyrin at 77K ($\tau = 0.11$ ms). This result suggests a quenching by photoinduced electron transfer, which is disfavored at 77 K because the solvent cannot reorganize and properly solvate the species produced upon charge separation.

Electrochemical measurements were performed to estimate the energy of the charge separated (CS) state obtained upon electron-transfer. Cyclic voltammetry of the supramolecular system $\mathbf{1}^{4+} \supset 4$Ru(CO)FTPP in CH_2Cl_2 solution in the presence of ferrocene as internal standard (Figure S35) shows a reduction at -0.55 V (versus SCE) and an oxidation at $+1.35$ V (versus SCE), which can be attributed to the tetramer reduction and the Ru(II) porphyrin oxidation, respectively, by comparison with the

electrochemistry of the individual components (see Supporting Information for more details). In the supramolecular assemblies $\mathbf{1}^{4+} \supset 4$Ru(CO)FTPP and $\mathbf{2}^{+} \supset$Ru(CO)FTPP the reduction of $\mathbf{1}^{4+}$ and $\mathbf{2}^{+}$, respectively, occurs at less negative potentials compared to the isolated species. On the contrary, the oxidation potential of Ru(CO)FTPP in the assembly is not significantly affected (Figure 7).[22]

Based on these results, the energy of the CS state was estimated at about 1.80 eV (Figure 8), that is, very close in energy to the lowest and emissive triplet state (T_1) of Ru(CO) TFPP ($E_{00} = 1.84$ eV).

In the $\mathbf{1}^{4+} \supset 4$Ru(CO)FTPP adduct (Figure 8), the fluorescent excited state S_1 of $\mathbf{1}^{4+}$ can be quenched (i) by electron transfer to populate the CS state or (ii) by energy transfer to populate the S_1 excited state of the porphyrin. The latter can also be populated by direct excitation in the Q-bands and deactivated through a very efficient intersystem crossing (isc) to the T_1 excited state promoted by the ruthenium heavy-atom effect.[30] Finally, the phosphorescent excited state T_1 of the porphyrin is quenched by electron transfer only at room temperature, while at 77 K no quenching occurs because of the expected increase of the CS state energy.
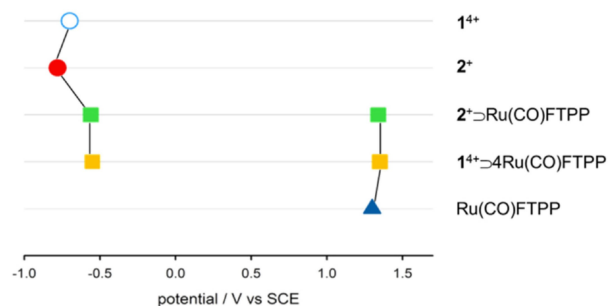
Figure 7. Comparison of the redox potentials of $\mathbf{1}^{4+}$ (light-blue empty circle, chemical irreversible process, E_{pc} at 0.2 V/s in CH_3CN), $\mathbf{2}^{+}$ (red circle, in CH_3CN), Ru(CO)FTPP (blue triangle, in CH_2Cl_2), $\mathbf{2}^{+} \supset$Ru(CO)FTPP (green squares, in CH_2Cl_2) and $\mathbf{1}^{4+} \supset$Ru(CO)FTPP (yellow squares, in CH_2Cl_2).

Chemistry–A European Journal

Full Paper
doi.org/10.1002/chem.202102135

**Chemistry
Europe**
European Chemical
Societies Publishing

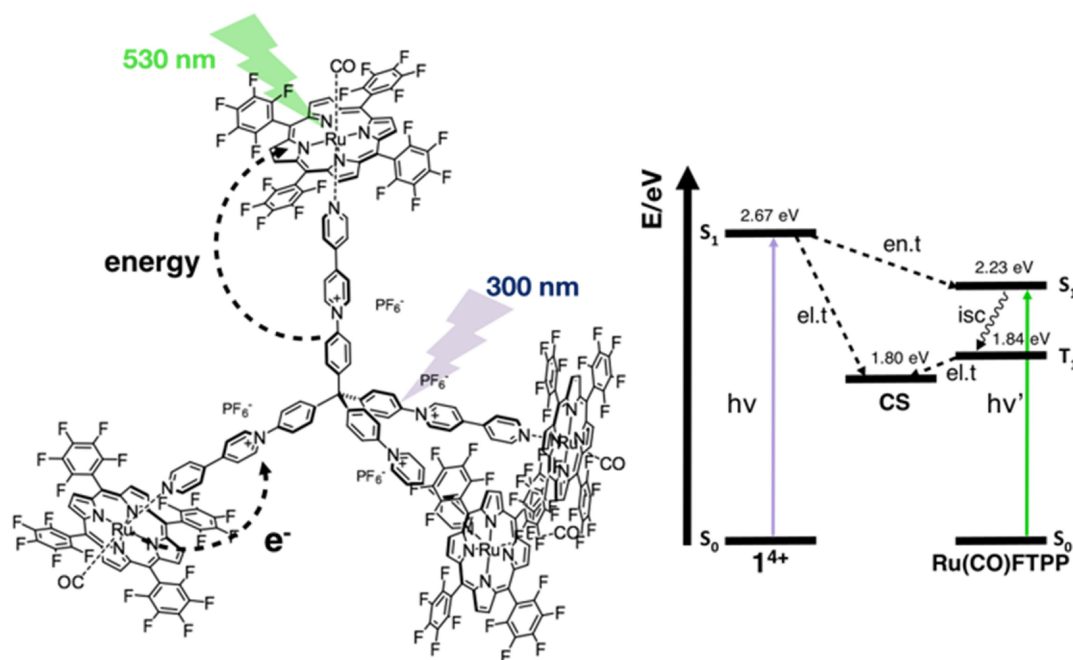**Figure 8.** A schematization of all the photophysical processes that can occur in the supramolecular assembly $1^{4+}\supset4$Ru(CO)FTPP.

In order to investigate in detail the photophysical processes occurring in the $1^{4+}\supset4$Ru(CO)FTPP adduct, pump-probe transient absorption measurements with femtosecond resolution were performed on the assembly and its model components 1^{4+} and Ru(CO)FTPP. For comparison, the analysis was also performed on the 1:1 adduct $2^{+}\supset$Ru(CO)FTPP and its models. Excitation was performed both at 550 nm, where the porphyrin is absorbing exclusively, and at 300 nm, where the pyridylpyridium units are predominantly excited.

Upon excitation at 550 nm, the spectral evolution of Ru(CO)FTPP (Figure S29) corresponds to the decay of the absorption of the lowest triplet excited state of the porphyrin, in agreement with literature reports.[31] The lifetime of the triplet excited state appears infinite on the time window of the experiment (maximum delay: 7 ns), in agreement with the value in the µs range measured for the porphyrin phosphorescence.

The scenario is completely different for $1^{4+}\supset4$Ru(CO)FTPP (Figure 9). A prompt signal rise of 25 ps is clearly observed in the 550–650 nm region, with a concomitant decay of the band at 474 nm. The spectrum that forms has characteristics of the porphyrin cation, such as absorption peaks between 600 and 800 nm and ground state bleaching at 530 nm[31] and of the reduced viologen species, that is, a broad band with maximum around 610 nm,[32] indicating the formation of the CS state. The latter decays to the ground state with a lifetime of ca. 800 ps. It is interesting to note that in the $2^{+}\supset$Ru(CO)FTPP adduct, after electron transfer, which occurs in ca. 25 ps, the CS state decays in 180 ps to a signal that remains stable on the time scale of the experiment, attributable to the porphyrin T_1 excited state (Figure S30). Charge recombination to the porphyrin triplet can be allowed by the energy proximity of the two states in this adduct, less favoured in the 1:4 system, where the delocaliza-
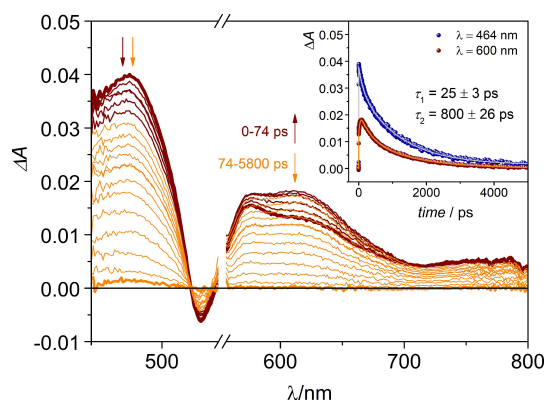

Figure 9. Transient absorption spectra of $1^{4+}\supset4$Ru(CO)FTPP in CH_2Cl_2 at the end-of-pulse (brown thick curve) and at different delays. Excitation at 550 nm ($A_{550}=0.20$, 0.2 cm optical path, 2 µJ/pulse). In the inset is reported the kinetic analysis at 464 nm and 600 nm.

tion of the electron over the whole tetrameric structure can lead to a stabilization of the CS state (Figure 8).

Excitation at 300 nm of the porphyrin model Ru(CO)FTPP results in a transient spectrum very similar to that obtained upon excitation at 550 nm (Figure S31). A bi-exponential decay, however, is observed in this case, with a short lifetime of 10 ps that precedes the long lifetime of the triplet excited state. The fast decay can be attributed to $S_2\rightarrow S_1$ internal conversion, being isc an ultrafast process.

The end-of-pulse spectrum of the tetramer 1^{4+} shows two positive bands at 450 nm and 515 nm and a negative band due to stimulated emission at 520 nm (Figure S32). This spectrum evolves into a broad signal that remains constant over the time span of the experiment, ascribable to the lowest triplet excited

Chemistry–A European Journal

Full Paper
doi.org/10.1002/chem.202102135

Chemistry Europe
European Chemical
Societies Publishing
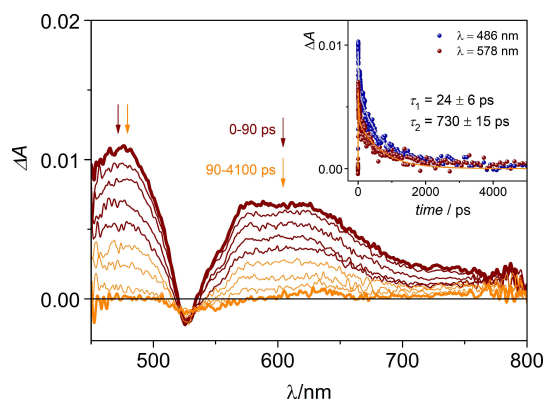
Figure 10. Transient absorption spectra of $1^{4+} \supset 4Ru(CO)FTPP$ in CH_2Cl_2 at the end-of-pulse (brown thick curve) and at different delays. Excitation at 300 nm ($A_{300} = 0.22$, 0.2 cm optical path, 2 μJ/pulse). In the inset is reported the kinetic analysis at 486 nm and 578 nm.

state. The decay of 1.25 ns well matches the measured fluorescence lifetime. The behaviour of model 2^+ is markedly different: the end-of-pulse spectrum, with a minimum at 492 nm (stimulated emission) and a positive broad absorption band peaking at 604 nm, evolves towards a spectrum showing a positive band slightly blue-shifted (Figure S33). The rise time of this process is 34 ps. The formed species then decays in 290 ps to form a new species with an absorption maximum at 472 nm. The latter spectrum is not further evolving in the time-span of the experiment and is ascribable to a triplet excited state. Indeed, the observed spectrum is similar to that reported for the triplet of 4–4'-bipyridine,[33] even if largely red-shifted. The lifetime of the second process, 290 ps, is in good accordance with the fluorescence lifetime measured for this compound. The initial process that precedes isc can be tentatively attributed to the formation of a charge transfer state, perhaps TICT-like (twisted intramolecular charge transfer) where the phenyl group acts as donor and the pyridinium unit as acceptor. In the larger and more constrained tetramer, this ultrafast process appears to be hindered.

Excitation of $1^{4+} \supset 4Ru(CO)FTPP$ leads to a spectrum that does not resemble the features of the models but already contains the bands characteristics of the CS state (Figure 10). The absence of a signal rise testifies that deactivation of the lowest singlet excited state of 1^{4+} is occurring within the instrumental time resolution ($\leq$ 300 fs), leading to population of both the CS state and the Ru(CO)FTPP singlet (Figure 8). The transient signal decays to zero with a bi-exponential behaviour, fitted with lifetimes of ca. 24 and 730 ps. They can be interpreted considering that the formed porphyrin singlet decays in 25 ps to yield the CS state (via the triplet level), and the value of 730 ps well agrees with the lifetime of ca. 800 ps observed for charge recombination upon excitation at 550 nm. The simpler 1:1 adduct behaves similarly, with an end-of-pulse spectrum containing CS features, decaying with lifetimes of ca. 20 ps and 180 ps to the porphyrin triplet state (Figure S34). The shorter lifetime can be attributed, similarly to the previous case, to the decay of the promptly formed porphyrin singlet and the

longer lifetime accounts for the charge recombination process, as detected upon excitation at 550 nm.

It can be noticed that, while forward electron transfer occurs with similar kinetics in both the 1:4 and the 1:1 adducts (ca. 25 ps from the porphyrin excited states), backward electron transfer is slower in the 1:4 system (800 ps vs. 180 ps), likely due to electron delocalization over the tetrameric pyridinium structure.

Conclusion

A shape persistent supramolecular array containing four ruthenium porphyrins and a central tetrapodal pyridilpyridinium moiety was prepared in high yield through self-assembly of the components in acetone. The system was fully characterized by NMR, UV-Vis spectroscopy, ultrafast transient absorption spectroscopy, single-crystal X-ray diffraction, and electrochemical measurements. These combined techniques proved that the targeted 1:4 stoichiometry of the adduct and the tetrahedral highly symmetric architecture was indeed the preferred supramolecular association motif between the selected components. Multinuclear NMR spectra suggest a highly symmetrical structure in solution, showing that the slow rotational dynamics of the phenyl moieties of the porphyrin macrocycle is retained in the tetrahedral assembly. The hydrodynamic radius measured from DOSY spectrum of the assembled system agrees with the molecular diameter derived from models and from that determined through X-ray single crystal analysis. The solid state structure, while confirming the formation of a tetrahedral giant multiporphyirn assembly, evidences the presence of some close contacts between the anions and the central charged scaffold. Spectrofluorimetric titrations confirm the 1:4 stoichiometry and evidence a complete quenching of both the bright fluorescence of the pyridylpyridinium scaffold and the weak phosphorescence of the Ru(II) porphyrin. This quenching process is a photoinduced electron transfer occurring at room temperature, as demonstrated by ultrafast transient absorption measurements. The lifetime of the charge separated state is about 800 ps, that is, over four times longer than the model adduct $2^+ \supset Ru(CO)FTPP$. This shows a remarkable effect of multiple supramolecular interactions in stabilizing the CS state and prolonging the duration of the high energy transient species within the giant array. This work demonstrates that multichromophoric systems can be relatively easily self-assembled from pyridylpyridinum units and porphyrin constituents leading to structures characterized by highly predictable shape persistent architectures. Studies aimed at further extending this self-assembling motif, either by tuning the photo and electrochemical characteristics of the metalloporphyrin units or the nature of the counteranions, are underway.

Chemistry–A European Journal

Full Paper
doi.org/10.1002/chem.202102135

**Chemistry
Europe**
European Chemical
Societies Publishing

Experimental Section

Materials and methods: Chemicals were purchased from Sigma-Aldrich or Alfa Aesar and used without further purification, unless otherwise stated. Solvents for spectroscopic measurements were of spectroscopic grade, all other chemicals were of reagent grade quality, and used as received. 5,10,15,20-tetrakis(pentafluorophenyl) porphyrin (FTPP) and 2,3,6,7,12,13,16,17-octaethylporphyrin (OEP) were purchased from Frontier Scientific and Sigma-Aldrich, respectively. Ru(CO)(FTPP) and Ru(CO)(OEP) were prepared according to literature procedures.[34] All NMR spectra were recorded on a *Varian 500* spectrometer at room temperature, operating at 500 MHz for ^{1}H, at 125 MHz for ^{13}C and at 470.12 for ^{19}F. ^{1}H and ^{13}C chemical shifts were referenced to the peak of residual non-deuterated solvent ($\delta = 2.05$ ppm and 29.84 ppm for acetone-d_6); ^{19}F chemical shifts was referenced, to the internal standards CFCl$_3$ at 0.00 ppm. HOESY experiments were run for 24 h with 500 ms mixing time. ^{1}H-DOSY experiments were run at controlled temperature using the Bipolar Pulse Paired Stimulated Echo sequence with convection compensation of Varian VnmrJ 3.2 software, $\delta = 2$ ms, $G = 1130$–28261 G/cm, and variable Δ.[35] Processing was done with MestRe-Nova$^{\copyright}$ software.[36]

Crystal structure determination: Data collections were performed at the X-ray diffraction beamline (XRD1) of the Elettra Synchrotron, Trieste (Italy).

Deposition Number(s) 2089855 ([2$^+$⊃Ru(CO)FTPP][PF$_6$]), 2089854 ([2$^+$⊃Ru(CO)FTPP][PF$_6$]alt), 2089856 ([2$^+$⊃Ru(CO)OEP][PF$_6$]) and 2089853 ([1^{4+}⊃4Ru(CO)FTPP][PF$_6$]$_4$) contain(s) the supplementary crystallographic data for this paper. These data are provided free of charge by the joint Cambridge Crystallographic Data Centre and Fachinformationszentrum Karlsruhe Access Structures service.

Photophysical measurements: Absorption spectra in the 190–1100 nm range were recorded at room temperature in solutions contained in quartz cuvettes (optical pathlength 1 cm, Hellma®) by using a Perkin Elmer λ40 spectrophotometer. Fluorescence and phosphorescence emission and excitation spectra in the 250–900 nm range were recorded with a Perkin Elmer LS 55 spectro-fluorimeter equipped with Hamamatsu R928 photomultiplier. Room temperature spectra were recorded in spectrofluorometric suprasil quartz cuvettes with 1 cm optical path. Lifetimes from 0.5 ns to 10 μs were measured by an Edinburgh FLS920 spectrofluorimeter equipped with a TCC900 card for data acquisition in time-correlated single-photon counting experiments (0.5 ns time resolution) with a pulsed diode laser. Lifetimes in the range between 10 μs and 5 s were measured with the same Perkin Elmer LS 50 spectrofluorim-eter upon excitation with a pulsed Xe lamp (repetition frequency: 5–50 Hz). Emission spectra in frozen matrix at 77 K were recorded using quartz (or glass) tubes with an internal diameter of about 2 mm and a 20 cm length immersed in liquid nitrogen. A trans-parent dewar (glass or quartz) with a cylindrical terminal part with a 1 cm external diameter was employed. The device fits into the sample holder of the spectrofluorimeters mentioned above. Meas-urements of emission spectra and lifetimes as a function of temperature were performed by inserting a quartz cell into a cryostat equipped with a temperature controller (model TC1) by Oxford Instruments.

Pump-probe transient absorption measurements were performed with an Ultrafast Systems HELIOS (HE-VIS-NIR) femtosecond tran-sient absorption spectrometer by using, as excitation source, a Newport Spectra Physics Solstice-F-1 K-230 V laser system, com-bined with a TOPAS Prime (TPR-TOPAS-F) optical parametric amplifier (pulse width: 100 fs, 1 kHz repetition rate) tuned at 300 nm and 550 nm. The overall time resolution of the system is 300 fs. Air-equilibrated solutions in 0.2 cm optical path quartz cells

were analyzed under continuous stirring. To reduce photo-degrada-tion, the pump energy on the sample was reduced to 2 μJ/pulse. Surface Xplorer V4 software from Ultrafast Systems was used for data acquisition and analysis. The 3D data surfaces were corrected for the chirp of the probe pulse prior to analysis.

Electrochemical measurements: CV scans were carried out in argon-purged acetonitrile and CH$_2$Cl$_2$ (Romil Hi-DryTM) solutions at room temperature with an EcoChemie Autolab 30 multipurpose instrument interfaced to a personalcomputer. The working elec-trode was a glassy carbon electrode (0.08 cm^2, Amel); the counter electrode was a Pt spiral and a silver wire was employed as a quasi-reference electrode (QRE). The potentials reported are referred to SCE by measuring the potential with respect to ferrocene ($+$ 0.395 V in acetonitrile; $+0.460$ V in CH$_2$Cl$_2$) or decamethyl ferrocene (-0.086 V in CH$_2$Cl$_2$). The substrate concentrations were in 10^{-3}–10^{-4} M range; a 0.1 M of supporting electrolyte (TBAPF$_6$) was also present. Cyclic voltammograms were obtained with scan rate of 0.2 V/s or 0.5 V/s.

Synthesis and characterization: [2$^+$⊃Ru(CO)FTPP][PF$_6$]. In a 5 mm NMR tube, 2.1 mg of [2$^+$][PF$_6$] (0.005 mmol) were dissolved in 0.65 ml of acetone-d_6. Small quantities of Ru(CO)FTPP were subsequently added till the total consumption of 2$^+$ was ascertained by ^{1}H NMR experiments. The solution was then trans-ferred in a 20 mL Pyrex tube and a layer of *n*-hexane was slowly added to induce precipitation by slow diffusion. The crystalline red product was filtered, washed with *n*-hexane and cool diethyl ether, and dried under vacuum. Yield 7.2 mg (88%). Alternatively, the product can be isolated, in a similar yields, *albeit* in larger amounts from 1:1 reaction of [2$^+$][PF$_6$] and Ru(CO)FTPP dissolved in acetone, followed by addition of *n*-hexane after 30 min. ^{1}H NMR (500 MHz, acetone-d_6, δ, ppm): 9.12 (d, $J_3 = 7.3$ Hz, 2H, py4), 9.09 (s, 8H, Hβ), 7.98 (d, $J_3 = 7.3$ Hz, 2H, py3), 7.52 (m, 5H, *o*H+*m*H+*p*H), 6.23 (d, $J_3 = 7.0$ Hz, 2H, py2), 1.74 (d, $J_3 = 7.0$ Hz, 2H, py1). ^{13}C NMR (HSQC, 125 MHz, acetone-d_6, δ, ppm): 144.50 (py1), 144.12 (py4), 132.10 (Hβ), 131.85–130.26 (*m*H+*p*H), 124.55 (py3), 123.98 (*o*H), 119.81 (py2). ^{19}F NMR (470.12 MHz, acetone-d_6, δ, ppm): -72.70 (d, $J_{FP} = 707.3$ Hz, 6F, PF$_6$) -139.78 (dd, $J_3 = 24.1$ Hz, $J_4 = 7.5$ Hz, 8F, *o*F$_{out}$) -140.73 (dd, $J_3 = 24.0$ Hz, $J_4 = 7.5$ Hz, 8F, *o*F$_{in}$) -155.96 (t, $J_3 = 20.4$ Hz, 86F, *p*F) -164.45 (td, $J_3 = 21.7$ Hz, $J_4 = 7.8$ Hz, 8F, *m*F$_{out}$) -165.13 (td, $J_3 = 21.7$ Hz, $J_4 = 7.8$ Hz, 8F, *m*F$_{in}$). Single crystals suitable for X-Ray diffraction were obtained from acetone/*n*-hexane solutions as bright orange needles or thin plates.

[1^{4+}⊃4Ru(CO)FTPP]$_4$[PF$_6$]$_4$ In a 5 mm NMR tube, 1.9 mg of [1^{4+}][PF$_6$]$_4$ (0.0013 mmol) were dissolved in 0.65 ml of acetone-d_6. Small quantities of Ru(CO)FTPP were subsequently and the consumption of [py4][PF$_6$]$_4$ was monitored after each addition by ^{1}H NMR experiments, until the proton resonances of free 1^{4+} were no longer detectable. The solution was then transferred in a 20 ml Pyrex tube and a layer of *n*-hexane was slowly added to induce precipitation by slow diffusion. The red crystalline product was filtered, washed with *n*-hexane and cool diethyl ether, and dried under vacuum. Yield 6.8 mg (92%). Alternatively, the product can be isolated, in a similar yields, *albeit* in larger amounts from 1:4 reaction of [1^{4+}][PF$_6$]$_4$ and Ru(CO)FTPP dissolved in acetone, followed by addition of *n*-hexane after 30 min. ^{1}H NMR (500 MHz, acetone-d_6, δ, ppm): 9.04 (s, 32H, Hβ), 8.80 (d, $J_3 = 7.1$ Hz, 8H, py4), 7.78 (d, $J_3 = 7.1$ Hz, 8H, py3), 7.47 (d, $J_3 = 8.9$ Hz, 8H, *o*H), 7.35 (d, $J_3 = 8.9$ Hz, 8H, *m*H), 6.11 (d, $J_3 = 6.9$ Hz, 8H, py2), 1.66 (d, $J_3 = 7.0$ Hz, 8H, py1). ^{13}C NMR (HSQC, 125 MHz, acetone-d_6, δ, ppm): 144.50 (py1), 144.42 (py4), 132.80 (Hβ), 131.95 (*m*H), 125.25 (py3), 124.20 (*o*H), 120.41 (py2). ^{19}F NMR (470.12 MHz, acetone-d_6, δ, ppm): -72.64 (d, $J_{FP} = 708.5$ Hz, 24F, PF$_6$) -139.81 (dd, $J_3 = 23.5$ Hz, $J_4 = 6.7$ Hz, 16F, *o*F$_{out}$) -140.70 (dd, $J_3 = 23.8$ Hz, $J_4 = 6.7$ Hz, 16F, *o*F$_{in}$) -156.02 (t, $J_3 = 20.6$ Hz, 16F, *p*F) -164.50 (td, $J_3 = 23.4$ Hz, $J_4 = 8.0$ Hz, 16F, *m*F$_{out}$) -165.17 (td, $J_3 = 23.6$ Hz, $J_4 = 8.0$ Hz, 16F, *m*F$_{in}$). Single crystals

Chemistry–A European Journal

Full Paper
doi.org/10.1002/chem.202102135

Chemistry Europe
European Chemical
Societies Publishing

suitable for X-Ray diffraction were obtained from acetone/*n*-hexane solutions and appeared as small, bright orange plates prone to radiation damage.

[**2**⁺⊃Ru(CO)OEP][PF₆]. In a 5 mm NMR tube, 1.7 mg of [**2**⁺][PF₆] (0.004 mmol) were dissolved in 0.65 ml of acetone-d_6. Small quantities of Ru(CO)OEP were subsequently added till the total consumption of **2**⁺ was ascertained by ¹H NMR experiments. The solution was then transferred in a 20 ml Pyrex tube and a layer of n-hexane was to induce precipitation by slow diffusion. The red crystalline product thus formed was filtered, washed with n-hexane and cool diethyl ether, and dried under vacuum. Yield: 4.23 mg (91%). Alternatively, the product can be isolated, in a similar yields, *albeit* in larger amounts from 1:1 reaction of [**2**⁺][PF₆] and Ru(CO)OEP dissolved in acetone, followed by addition of *n*-hexane after 30 min. ¹H NMR (500 MHz, acetone-d_6, δ, ppm): 10.05 (s, 4H, Hmeso), 8.98 (d, $J_3 = 6.8$ Hz, 2H, py4), 7.70 (d, $J_3 = 6.8$ Hz, 2H, py3), 7.62 (m, 5H, oH + mH + pH), 5.82 (d, $J_3 = 6.3$ Hz, 2H, py2), 4.08 (m, 8H, CH₂), 1.93 (t, $J_3 = 7.6$ Hz, 12H, CH₃), 1.18 (d, $J_3 = 6.3$ Hz, 2H, py1). ¹³C NMR (HSQC, 125 MHz, acetone-d_6, δ, ppm): 145.05 (py1), 144.55 (py4), 131.52–130.26 (mH + pH), 125.16 (py3), 124.19 (oH), 119.45 (py2), 98.10 (Hmeso), 19.14 (CH₂), 17.91 (CH₃). Single crystals suitable for X-Ray analysis were obtained from acetone/n-hexane solutions, as deep purple needles.

[**1**⁴⁺⊃4Ru(CO)OEP]₄[PF₆]₄. In a 5 mm NMR tube, 2.3 mg of [**1**⁴⁺][PF₆]₄ (0.0015 mmol) were dissolved in 0.65 mL of acetone-d_6. Small quantities of Ru(CO)OEP were subsequently added till the total consumption of **1**⁴⁺ was ascertained by ¹H NMR experiments. The solution was then transferred in a 20 ml Pyrex tube and a layer of n-hexane was slowly added to induce precipitation by slow diffusion. The product was filtered, washed with n-hexane and cool diethyl ether, and dried under vacuum. Yield 5.1 mg (81%). Alternatively, the product can be isolated, in a similar yields, *albeit* in larger amounts from 1:4 reaction of [**1**⁴⁺][PF₆]₄ and Ru(CO)OEP dissolved in acetone, followed by addition of *n*-hexane after 30 min. ¹H NMR (500 MHz, acetone-d_6, δ, ppm): 9.99 (s, 16H, Hmeso), 8.66 (d, $J_3 = 6.6$ Hz, 8H, py4), 7.49 (d, $J_3 = 6.6$ Hz, 8H, py3), 7.38 (d, $J_3 = 8.8$ Hz, 8H, oH), 7.25 (d, $J_3 = 8.7$ Hz, 8H, mH), 5.68 (d, $J_3 = 6.7$ Hz, 8H, py2), 4.02 (m, 64H, CH₂), 1.88 (t, $J_3 = 7.5$ Hz, 96H, CH₃), 1.08 (d, $J_3 = 6.7$ Hz, 8H, py1). ¹³C NMR (HSQC, 125 MHz, acetone-d_6, δ, ppm): 145.05 (py1), 144.15 (py4), 131.92 (mH), 124.99 (py3), 124.08 (oH), 119.31 (py2), 98.04 (Hmeso), 19.10 (CH₂), 17.86 (CH₃).

Conflict of Interest

The authors declare no conflict of interest.

[1] a) W. Zhang, J. S. Moore, *Angew. Chem. Int. Ed.* **2006**, *45*, 4416–4439; *Angew. Chem.* **2006**, *118*, 4524–4548; b) J. S. Moore, *Acc. Chem. Res.* **1997**, *30*, 402–413.

[2] a) Q. Wang, Y. Zhong, D. P. Miller, X. Lu, Q. Tang, Z.-L. Lu, E. Zurek, R. Liu, B. Gong, *J. Am. Chem. Soc.* **2020**, *142*, 2915–2924; b) T.-T.-T. Nguyen, D. Türp, D. Wang, B. Nölscher, F. Laquai, K. Müllen, *J. Am. Chem. Soc.* **2011**, *133*, 11194–11204; c) C. Giansante, V. Balzani, P. Ceroni, M. Venturi, J. Sakamoto, A. D. Schlüter, *Chem. Eur. J.* **2008**, *14*, 10772–10781; d) J.-L. Wang, J. Yan, Z.-M. Tang, Q. Xiao, Y. Ma, J. Pei, *J. Am. Chem. Soc.* **2008**, *130*, 9952–9962.

[3] J. Iehl, M. Frasconi, H. P. Jacquot de Rouville, N. Renaud, S. M. Dyar, N. L. Strutt, R. Carmieli, M. R. Wasielewski, M. A. Ratner, J. F. Nierengarten, J. F. Stoddart, *Chem. Sci.* **2013**, *4*, 1462–1469.

[4] C. M. Ronconi, J. F. Stoddart, V. Balzani, M. Baroncini, P. Ceroni, C. Giansante, M. Venturi, *Chem. Eur. J.* **2008**, *14*, 8365–8373.

[5] V. Balzani, H. Bandmann, P. Ceroni, C. Giansante, U. Hahn, F.-G. Klärner, U. Müller, W. M. Müller, C. Verhaelen, V. Vicinelli, F. Vögtle, *J. Am. Chem. Soc.* **2006**, *128*, 637–648.

[6] V. Balzani, P. Ceroni, C. Giansante, V. Vicinelli, F.-G. Klärner, C. Verhaelen, F. Vögtle, Uwe Hahn, *Angew. Chem. Int. Ed.* **2005**, *44*, 4574–4578; *Angew. Chem.* **2005**, *117*, 4650–4654.

[7] F. Marchioni, M. Venturi, P. Ceroni, V. Balzani, M. Belohradsk, A. M. Elizarov, H.-R. Tseng, J. F-Stoddart, *Chem. Eur. J.* **2004**, *10*, 6361–6368.

[8] S. Heinen, L. Walder, *Angew. Chem. Int. Ed.* **2000**, *39*, 806–809; *Angew. Chem.* **2000**, *112*, 811–814.

[9] Y. Wang, J. Sun, Z. Liu, M. S. Nassar, Y. Y. Botros, J. F. Stoddart, *Chem. Sci.* **2017**, *8*, 2562–2568.

[10] H. R. Wessels, C. Slebodnick, H. W. Gibson, *J. Am. Chem. Soc.* **2018**, *140*, 7358–7370.

[11] E. Coronado, P. Gaviña, Sergio Tatay, *Chem. Soc. Rev.* **2009**, *38*, 1764–1689.

[12] A. Coskun, M. Banaszak, R. D. Astumian, J. F. Stoddart, B. A. Grzybowski, *Chem. Soc. Rev.* **2012**, *41*, 19–30.

[13] Y. Alesanco, J. Palenzuela, R. Tena-Zaera, G. Cabañero, H. Grande, B. Herbig, A. Schmitt, M. Schott, U. Posset, A. Guerfi, M. Dontigny, K. Zaghib, A. Viñuales, *Sol. Energy Mater. Sol. Cells* **2018**, *157*, 624–635.

[14] R. J. Mortimer, T. S. Varley, *Chem. Mater.* **2011**, *23*, 4077–4082.

[15] S. Sen, J. Saraidaridis, S. Y. Kim, G. T. R. Palmore, *ACS Appl. Mater. Interfaces* **2013**, *5*, 7825–7830.

[16] S. Wang, W. J. Oldham, R. A. Hudack, G. C. Bazan, *J. Am. Chem. Soc.* **2010**, *122*, 5695–5709.

[17] T. Lin, X.-M. Liu, C. He, *J. Phys. Chem. B* **2004**, *108*, 17361–17368.

[18] M. Mastalerz, I. M. Oppel, *Eur. J. Org. Chem.* **2011**, 5971–5980.

[19] I. Aujard, J.-P. Baltaze, J.-B. Baudin, E. Cogné, F. Ferrage, L. Jullien, É. Perez, V. Prévost, L. M. Qian, O. Ruel, *J. Am. Chem. Soc.* **2001**, *123*, 8177–8188.

[20] a) K. Funatsu, T. Imamura, A. Ichimura, Y. Sasaki, *Inorg. Chem.* **1998**, *37*, 1798–1804; b) J. K. M. Sanders, N. Bampos, Z. Clyde Watson, S. L. Darling, J. C. Hawley, H–J. Kim, C. C. Mak, S. J. Webb, *The Porphyrin Handoboox*, **2003**, *3*, 15–48, K. M. Kadish, K. M. Smith, R. Guilard Eds; c) I. Beletskaya, V. S. Tyurin, A. Y. Tsivadze, R. Guillard, C. Stern, *Chem. Rev.* **2009**, *109*, 1659–1713; d) M. Krempe, R. Lippert, F. Hampel, I. Ivanovic-Burmazovic, N. Jux, R. R. Tykwinski, *Angew. Chem. Int. Ed.* **2016**, *55*, 14802–14806; *Angew. Chem.* **2016**, *128*, 15022–15026.

[21] a) F. Scandola, C. Chiorboli, A. Prodi, E. Iengo, E. Alessio, *Coord. Chem. Rev.* **2006**, *250*, 1471–1496; b) A. Prodi, C. Chiorboli, F. Scandola, E. Iengo, E. Alessio, R. Dobrawa, F. Würthner, *J. Am. Chem. Soc.* **2005**, *127*, 1454–1462; c) E. Iengo, G. D. Pantoş, J. K. M. Sanders, M. Orlandi, C. Chiorboli, S. Fracasso, F. Scandola, *Chem. Sci.* **2011**, *2*, 676–685; d) A. Amati, M. Natali, M. T. Indelli, E. Iengo, F. Würthner, *ChemPhysChem* **2019**, *20*, 2195–2203.

[22] In parallel, the self-assembled multi-porphyrin system **1**⁴⁺⊃4Ru(CO)OEP (Ru(CO)OEP = 2,3,6,7,12,13,16,17-octaethyl-ruthenium(II)carbonyl-porphyrin) alongside with its model compound **2**⁺⊃Ru(CO)OEP, were prepared (see Scheme S2 and Experimental Section) and fully characterized. Solution NMR, UV-Vis absorption, emission and electrochemical data for **1**⁴⁺⊃4Ru(CO)OEP and **2**⁺⊃Ru(CO)OEP are reported in the Supporting Information. Single crystal X-ray analysis for [**2**⁺⊃Ru(CO)OEP][PF₆] is also provided in the Supporting Information.[23]

[23] For all derivatives, two alternative formulations that takes or not into account the presence of PF_6^- counterion(s) are used, depending on the whether the presence of the anion(s) is relevant to the discussion.

[24] a) K. Chichak, N. R. Branda, *Chem. Commun.* **1999**, 523–524; b) K. Campbell, R. McDonald, N. R. Branda, R. R. Tykwinski, *Org. Lett.* **2001**, *3*, 1045–1048; c) Y. Gao, V. Walter, M. J. Ferguson, R. R. Tykwinski, *Chem. Eur. J.* **2020**, *26*, 16712–16720.

[25] The rotation of the porphyrin *meso* aryl rings is slow on the NMR time scale, with the two halves of the rings becoming not equivalent, for RuII (CO)-porphyrins because of the presence of the strongly bound CO moiety on one side of the porphyrin. This inequivalence is significantly enhanced in the presence of axially N-bound ligands on the sixth coordination site of the ruthenium center (this latter is normally occupied by one loosely bound EtOH molecule in the isolated metalloporphyrin).[20,21,24]

[26] Attempts to obtain mass data performed with the indoor electrospray instrument were unsuccessful, and only afforded spectral patterns corresponding to fragmentation in the building components. Loss of the Ru[II](CO)-porphyrin units in such type of side-to-face assemblies is often encountered..[21c,24c]

[27] A. Macchioni, G. Ciancaleoni, C. Zuccaccia, D. Zuccaccia, *Chem. Soc. Rev.* **2008**, *37*, 479–489.

[28] Weighted average lifetime as a result of a biexponential fitting.

[29] G. Bergamini, A. Fermi, M. Marchini, M. Locritani, A. Credi, M. Venturi, F. Negri, P. Ceroni, M. Baroncini, *Chem. Eur. J.* **2014**, *20*, 7054–7060.

[30] A. A. Lamola, G. S. Hammond, *J. Chem. Phys.* **1965**, *43*, 2129–2135.

[31] E. Iengo, G. D. Pantoş, J. K. M. Sanders, M. Orlandi, C. Chiorboli, S. Fracasso, F. Scandola, *Chem. Sci.* **2011**, *2*, 676–685.

[32] a) J. Peon, X. Tan, J. D. Hoerner, C. Xia, Y. Fei Luk, B. Kohler, *J. Phys. Chem. A* **2001**, *105*, 5768–5777; b) T. Häupl, R. Lomoth, L. Hammarström, *J. Phys. Chem. A* **2003**, *107*, 435–438.

[33] a) F. Elisei, U. Mazzucato, H. Görner, D. Schulte-Frohlinde, *J. Photochem. Photobiol. A* **1989**, *50*, 209–219; b) G. Buntinx, P. Valat, V. Wintgens, O. Poizat, *J. Phys. Chem.* **1991**, *95*, 9347–9352.

[34] V. Marvaud, A. Vidal-Ferran, S. J. Webb, J. K. M. Sanders, *Dalton Trans.* **1997**, *24*, 985–990.

[35] D. H. Wu, A. D. Chen, C. S. Johnson, *J. Magn. Reson. Ser. A* **1995**, *115*, 260–264.

[36] *MestReNova© software, version 6.0.2, Mestrelab Res. S. L.*, Santiago Compost. Spain **2009**.